

project name (acronym): X. Gaps and Rings with Planet Scenario

S. ZHANG, Z. ZHU, ...¹

¹Department of Physics and Astronomy, University of Nevada, Las Vegas, 4505 S. Maryland Pkwy, Las Vegas, NV, 89154, USA

ABSTRACT

TBD

Keywords: circumstellar matter — planetary systems: formation, protoplanetary disks — dust

1. INTRODUCTION

generic background: to understand planet formation, we need to find young forming planets in protoplanetary disks. However, direct detection is difficult and we only have 6 candidates so far. Indirect methods which use disk features induced by planet-disk interaction can be efficient at probing young planets.

Planet-disk interaction has been studied thoroughly over the past three decades. Analytical models, 2 dimensional, 3 dimensional models have all been developed. However, earlier works focus on planet migration and gap opening. Only very recently, with the striking ALMA images, people have started to focus on studying the detectability of disk features due to planet-disk interaction. Most efforts have been studying features from dust scattering (near-IR scattered light images, submm polarization) or dust thermal emission (submm emission). Recently, people start to use gas kinematics to probe planets (sub/super Keplerian motion and velocity kinks).

Among all these methods, probing dust submm emission is still the most sensitive method to low planets planet since little gas surface density can cause dramatic dust surface density change. However, there is huge degeneracy and a lot of mechanisms can cause dust rings/gaps, such as ice lines, dead zone transition, MHD zonal flows, dust gravitational instability, resonances with planets, etc.

However, there is no systematic study on thermal emission features due to planet-disk interaction among different disk properties and planet properties. In this work, we did such parameter study. Our work differs from previous work in several aspects.

2. METHOD

We carried out 2-D hydrodynamical simulations using the modified version of the grid-based code FARGO, called FARGO-particle. It simulate gas hydrodynamics using finite difference method, while simulate the dust dynamics using Lagrangian particle method.

2.1. Setup: Gas and Dust

To represent the surface density of a realistic disk, we initialize the gas surface density as

$$\Sigma(r) = \Sigma_0(R/R_0)^{-1}, \quad (1)$$

where $R_0=1$. Isothermal EOS, grid range, resolution, boundary condition, indirect force, smoothing length, (basically parameters in the input file)... .

The dust's total surface density is 1/100 of the gas surface density. No disk self-gravity, no gas gravity from gas to dust. no feedback. All these to ensure that we can scale the simulations.

The dust particles are much smaller than the molecular mean-free path in our disk model so that the drag force experienced by the particles is in the Epstein regime. The dimensionless stopping time

$$St = t_s \Omega = \frac{\pi}{2} \frac{s \rho_p}{\Sigma_{gas}} \quad (2)$$

If we use $\rho_p = 1 g cm^{-3}$, we have

$$St = \dots \quad (3)$$

We use x0,000 particles. Each particle is a super particle. The dust size distribution. particle turbulent diffusion.

2.2. Grid of Models

We chose three h/r ($h/r=0.05, 0.07, 0.1$), 5 planet mass ($3.3 \times 10^{-5}, 10^{-4}, 3.3 \times 10^{-4}, 10^{-3}, 3.3 \times 10^{-3} M_\odot$ or roughly $11 M_\oplus, 33 M_\oplus, 0.35 M_J, 1 M_J, 3.5 M_J$), and 3 disk viscosity α ($\alpha = 0.1, 0.01, 0.001$).

The reason to choose these parameters....

Acronym h5am3p1 means $h/r=0.05, \alpha = 10^{-3}, M_p = 3.3 \times 10^{-5} M_\odot$.

2.3. Calculating the Intensity at Submm

How to scale the simulation results to real systems with a given star mass, luminosity, and surface density?

1) calculate the gas temperature using the new fitting formula.

2) use the estimated gas surface density to calculate how the particles size in real systems corresponds to particles in simulations.

3) Using the assumed particle size distribution in real system to calculate the mass weight for each particles in the simulation.

4) Add the opacity for each sized particle to derive the total optical depth.

5) Calculate $1 - \exp(-\tau)$, and derive the brightness temperature.

3. SIMULATION RESULTS

3.1. Gas

The azimuthally averaged gas surface density at $t=100 T_0$ for $h/r=0.05, 0.07$, and 0.1 cases are shown in Figure 1.

1) When the planet mass increases, the gap depth normally increases. However, when the gap is eccentric (e.g. h5am4p5, h5am3p5), the azimuthally averaged gas surface density is actually higher than the case with lower mass planets. This is purely due to the averaging process.

2) With the same planet mass, gaps in $h/r=0.1$ cases are shallower but wider than the $h/r=0.05$ cases. This is consistent with previous studies (Kanagawa et al. 2015, 2016).

3) With the same planet mass, the same h/r , the gaps are shallower with increasing α .

4) The gap edge becomes smoother with increasing α . With $\alpha = 0.01$, the gap edge is very smooth. With $\alpha = 10^{-3}$, the gap edge increases a little bit. With $\alpha = 10^{-4}$, clearly we see two spikes at the gap edge.

5) For $\alpha = 10^{-4}$ cases, we see multiple rings as in recent papers.

The two-dimensional contours in Figure 2 show a lot of details on the azimuthal structure of the disk.

3.2. Dust and Thermal Emission

Since dust to gas feedback is assumed to be not important, we can scale our dust distribution to match any system. To explore how different dust size distribution can affect the final intensity images, we choose two very different dust size distribution to explore the effect. In one case, we assume $n(s) \propto s^{-3.5}$ with the maximum grain size of 0.55 mm in the initial condition. And in the other case, we assume $n(s) \propto s^{-2}$ with the maximum grain size of 5.5 mm. The shallower dust size distribution is consistent with SED constraints (D'Alessio et al. 2001). The shallower slope and the bigger particle size explore the scenario that dust has grown in protoplanetary disks already.

The intensity for these two dust size distributions are shown in Figures 3 and 4.

With bigger particles, the gap edge is definitely sharper and forming a narrower ring. The larger the α is, the rings are wider.

Several non-axisymmetric structures to notice:

1) The gaps in the lower left plots (h5am4p5, h5am3p5) are eccentric. Eccentric gaps only show up

with massive planets. So maybe we can use gap eccentricity to constrain the planet mass.

2) For the lowest viscosity case ($\alpha = 10^{-4}$), vortices can appear at the gap edge. Even a $30 M_\odot$ planet can induce the vortex. The vortex sometimes is inside the gap edge. (probably it concentrates smaller particles while bigger particles are trapped outside further away at the gap edge. Needs to be checked)

3) The dust concentration at L4 or L5 or both L4/L5 is seen in some $\alpha = 10^{-4}$ cases.

Since the same sized particle has different dynamical properties (stokes number) with different disk gas surface density. We have explored three gas surface densities ($0.1, 1, 10 g/cm^2$).

4. FITTING GAPS/RINGS

We derive the gap depth and width in the intensity image for all cases.

We apply those to LP sources to derive the potential planet mass. We will do for all gaps. But we will caution that the deeper and wider gaps have higher chances to be associated with planets.

5. DISCUSSION

5.1. The Smallest Planets Probed by ALMA

We will explore what mass planets can be probed by ALMA. Provide the detection limit using dust continuum.

5.2. Our Solar System and HR 8799 in Taurus

If we put our solar system and HR 8799 in Taurus, how they look like?

6. CONCLUSION

7. APPENDIX

The fitting formula for all the gaseous gaps.

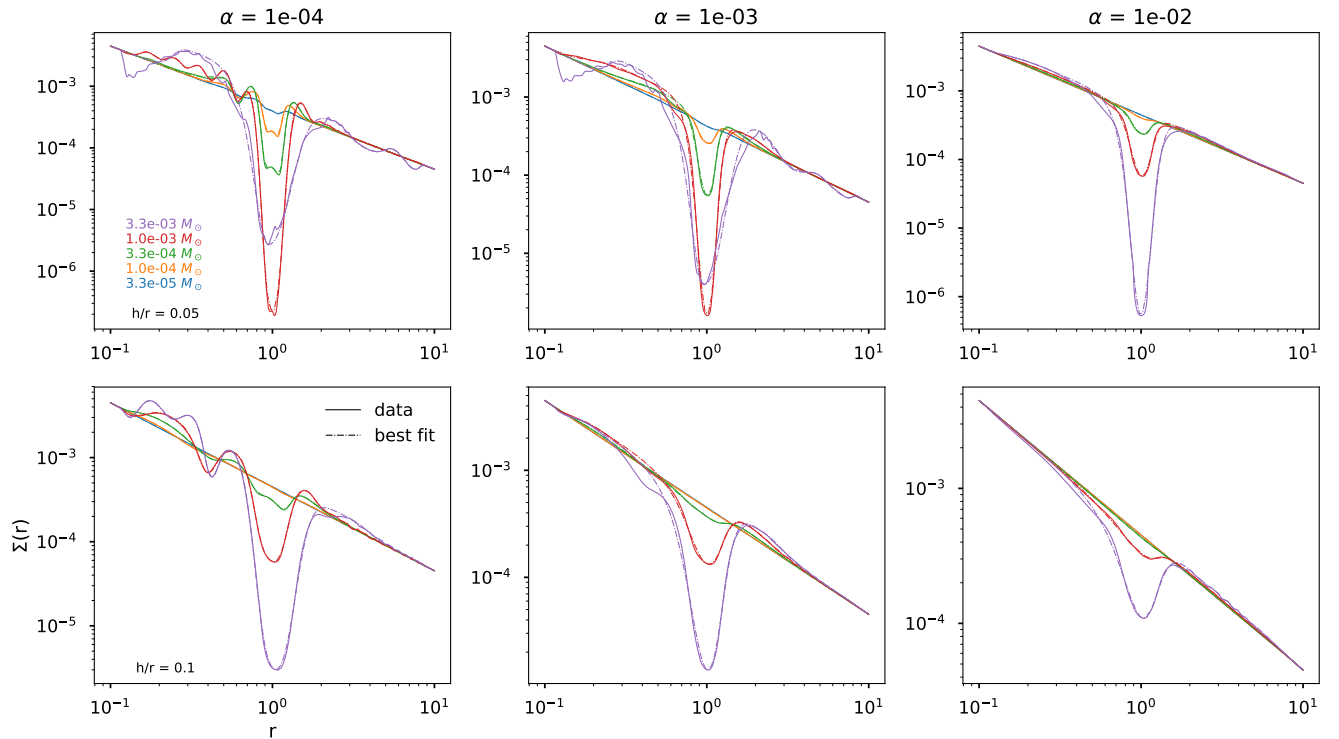


Figure 1. The gas surface density for $h/r=0.05$ cases (upper panels) and $h/r=0.1$ cases (bottom panels). From left to right, $\alpha = 10^{-4}, 10^{-3}, 10^{-2}$ in disks. Different colors represent planets having different masses.

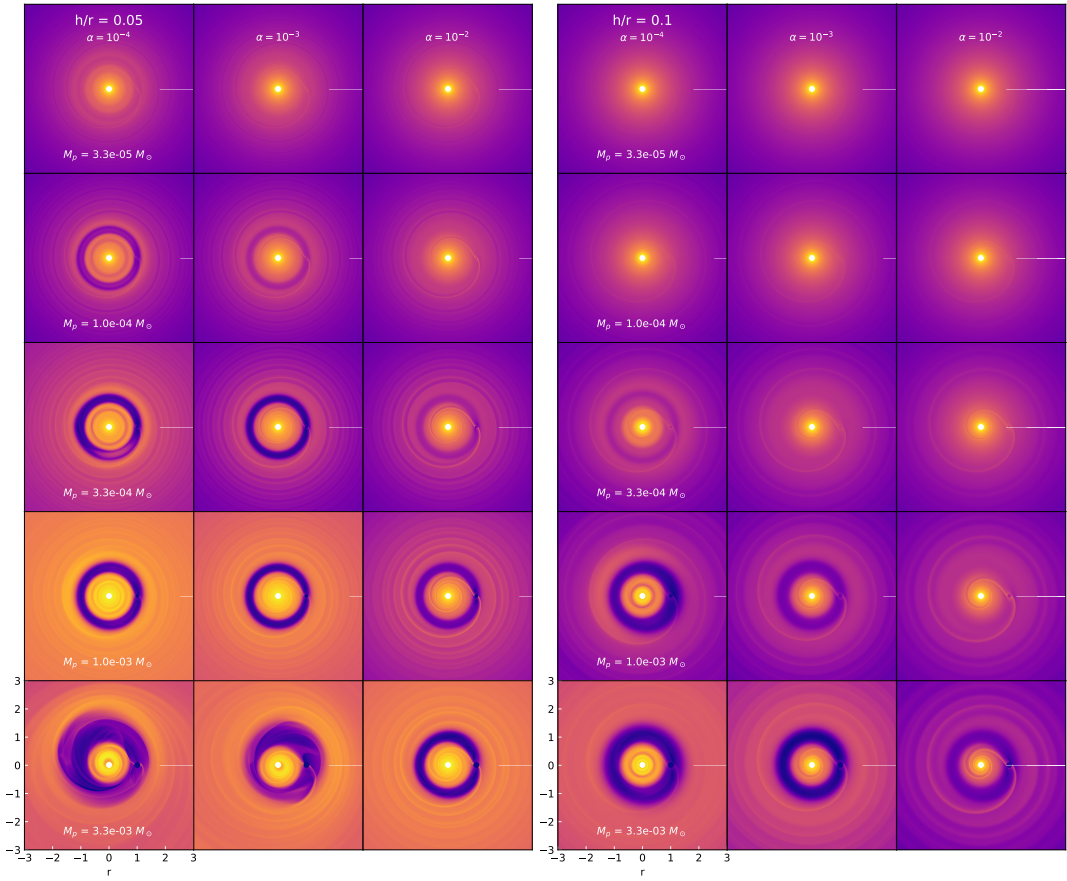


Figure 2. The gas surface density in log scale for $h/r=0.05$ cases (upper panels) and $h/r=0.1$ cases (bottom panels). From left to right, $\alpha = 10^{-4}, 10^{-3}, 10^{-2}$ in disks. The planet mass increases from top to bottom

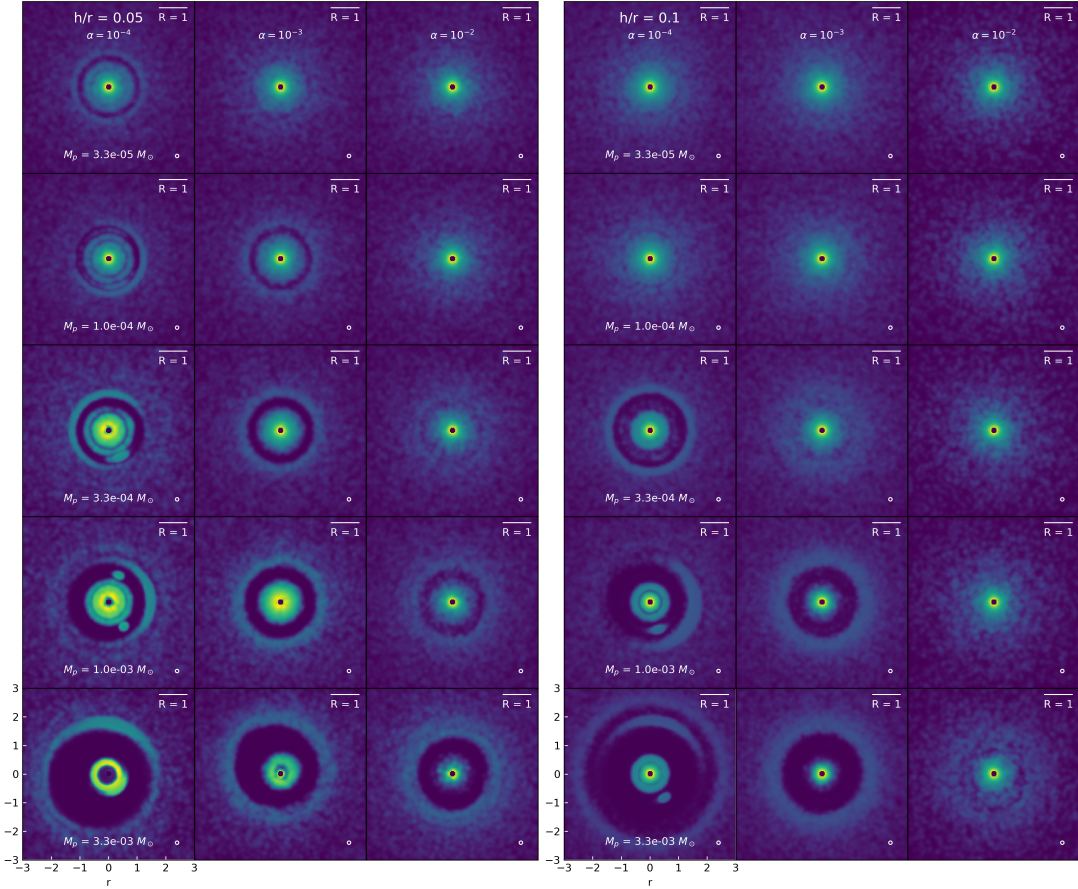


Figure 3. Similar to Figure 4, except that the initial dust size distribution follows $n(s) \propto s^{-3.5}$ with the maximum grain size of 0.55 mm.

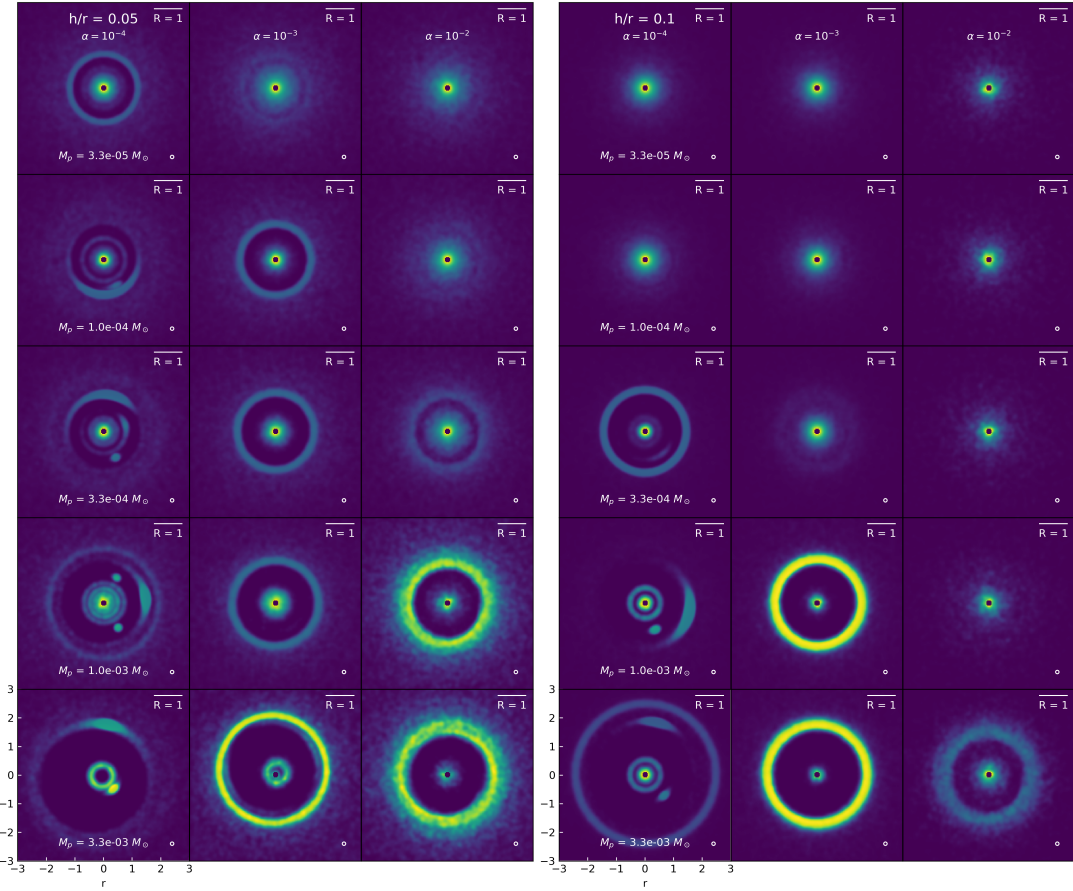


Figure 4. The intensity contours for cases with $h/r=0.05$ (left panels) and $h/r=0.1$ (right panels). The initial gas surface density at the planet position is 10 g cm^{-2} . From left to right, $\alpha = 10^{-4}, 10^{-3}, 10^{-2}$ in disks. From top to bottom, the planet masses increases. The initial dust size distribution is assumed to follow $n(s) \propto s^{-2}$ with the maximum grain size of 5.5 mm.

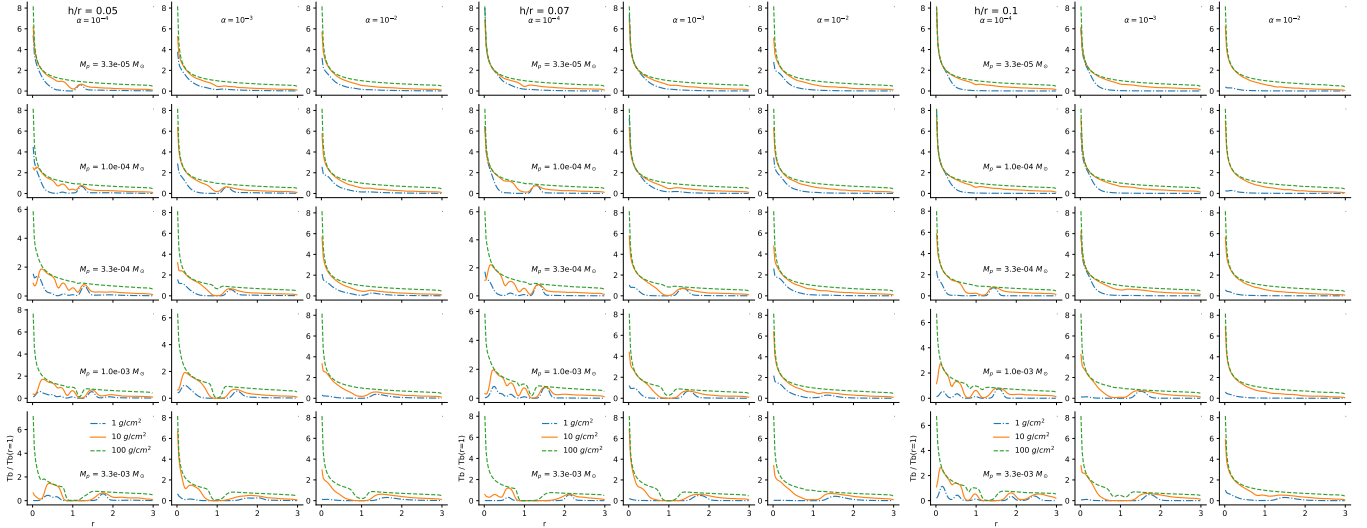


Figure 5. The radial intensity for cases with $h/r=0.05$ (left panels) and $h/r=0.1$ (right panels). The initial gas surface density at the planet position is 10 g cm^{-2} . From left to right, $\alpha = 10^{-4}, 10^{-3}, 10^{-2}$ in disks. From top to bottom, the planet masses increases. The upper three have the initial dust size distribution of $n(s) \propto s^{-3.5}$ with the maximum grain size of 0.55 mm. The lower three have the initial dust size distribution of $n(s) \propto s^{-2}$ with the maximum grain size of 5.5 mm.

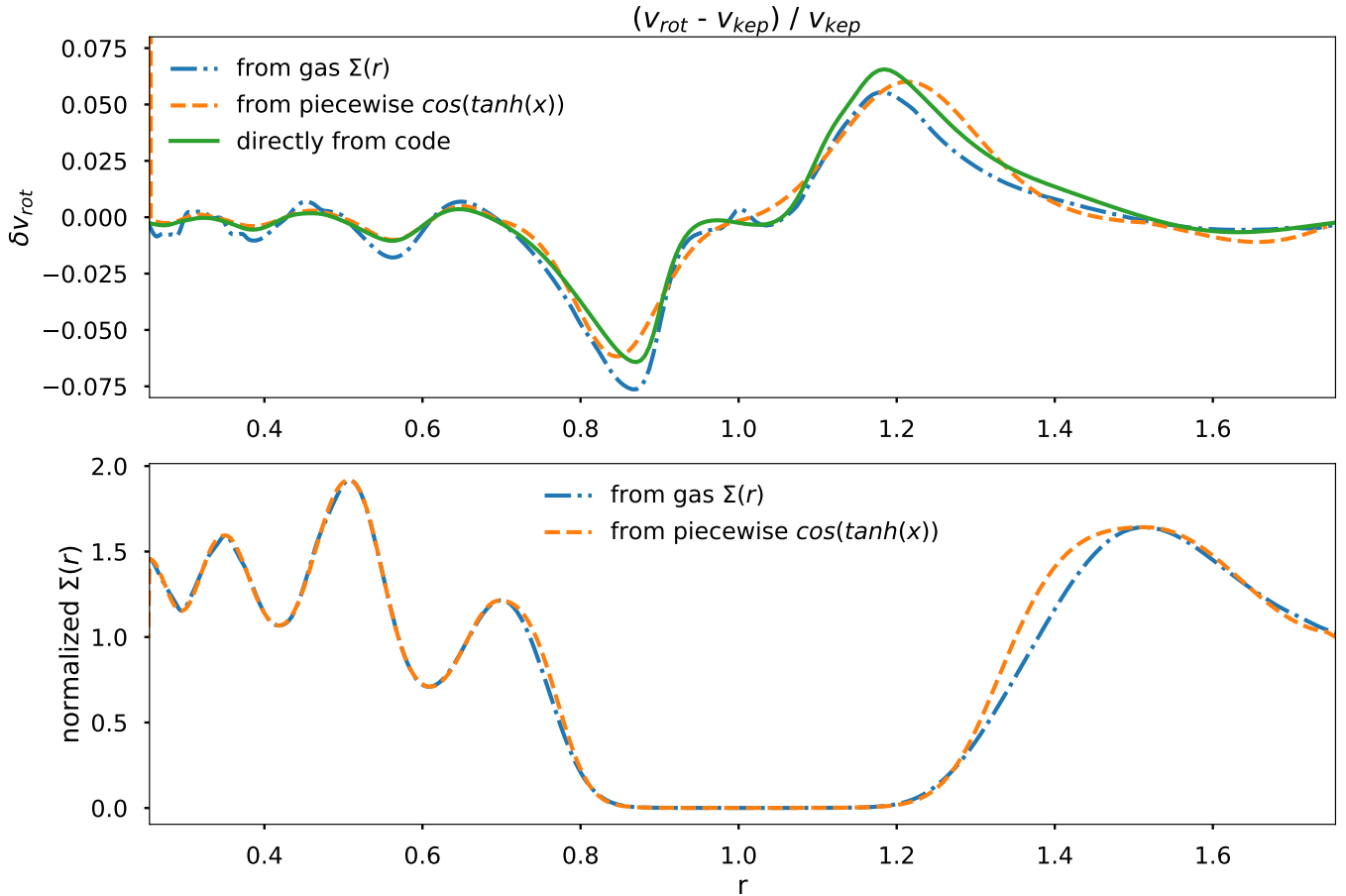


Figure 6. The azimuthal velocity from simulations and fittings.